Production of particle unstable light nuclei in 11.5*A* GeV/*c* Au+Pt heavy-ion collisions

T. A. Armstrong,[8,*] K. N. Barish,[3] S. Batsouli,[13] S. J. Bennett,[12] M. Bertaina,[7,†] A. Chikanian,[13] S. D. Coe,[13,‡] T. M. Cormier,[12] R. Davies,[9,§] C. B. Dover,[1,‖] P. Fachini,[12] B. Fadem,[5] L. E. Finch,[13] N. K. George,[13,¶] S. V. Greene,[11] P. Haridas,[7,**] J. C. Hill,[5] A. S. Hirsch,[9] R. Hoversten,[5] H. Z. Huang,[2] H. Jaradat,[12] B. S. Kumar,[13,††] T. Lainis,[10] J. G. Lajoie,[5] R. A. Lewis,[8] Q. Li,[12] B. Libby,[5,‡‡] R. D. Majka,[13] T. E. Miller,[11] M. G. Munhoz,[12] J. L. Nagle,[4] I. A. Pless,[7] J. K. Pope,[13,§§] N. T. Porile,[9] C. A. Pruneau,[12] M. S. Z. Rabin,[6] J. D. Reid,[11,‖‖] A. Rimai,[9,¶¶] A. Rose,[11] F. S. Rotondo,[13,a] J. Sandweiss,[13] R. P. Scharenberg,[9] A. J. Slaughter,[13] G. A. Smith,[8] M. L. Tincknell,[9,b] W. S. Toothacker,[8,‖] G. Van Buren,[7,2,c] F. K. Wohn,[5] and Z. Xu[13]

(The E864 Collaboration)

[1]*Brookhaven National Laboratory, Upton, New York 11973*
[2]*University of California at Los Angeles, Los Angeles, California 90095*
[3]*University of California at Riverside, Riverside, California 92521*
[4]*Columbia University, New York, New York 10027*
[5]*Iowa State University, Ames, Iowa 50011*
[6]*University of Massachusetts, Amherst, Massachusetts 01003*
[7]*Massachusetts Institute of Technology, Cambridge, Massachusetts 02139*
[8]*Pennsylvania State University, University Park, Pennsylvania 16802*
[9]*Purdue University, West Lafayette, Indiana 47907*
[10]*United States Military Academy, West Point, New York 10996*
[11]*Vanderbilt University, Nashville, Tennessee 37235*
[12]*Wayne State University, Detroit, Michigan 48201*
[13]*Yale University, New Haven, Connecticut 06520*

(Received 19 October 2000; revised manuscript received 13 July 2001; published 10 December 2001)

We report measurements from experiment E864 at the BNL-AGS of the yields of particle unstable light nuclei in central collisions of ^{197}Au with beam momentum of 11.5*A* GeV/*c* on ^{197}Pt. Yields are reported as a function of rapidity for the nuclei ^{4}H, ^{4}Li, ^{5}He, and ^{5}Li in the rapidity range from $y_{\mathrm{c.m.}}$ to $y_{\mathrm{c.m.}}+0.8$ and in the transverse momentum range of approximately $0.1 \leqslant p_T/A \leqslant 0.4$ GeV/c. The yields are compared to previously reported yields and trends for the production of stable light nuclei. The nonobservation of two excited states $^{5}\mathrm{He}^{*}_{16.75\ \mathrm{MeV}}$ and $^{5}\mathrm{Li}^{*}_{16.66\ \mathrm{MeV}}$ is used to set an upper limit on the yields of these states.

DOI: 10.1103/PhysRevC.65.014906 PACS number(s): 25.75.−q

I. INTRODUCTION

Relativistic heavy-ion collisions which are believed to reach energy densities many times greater than normal nuclear matter allow examination of the strong interaction in a novel environment. In order to understand the dynamics of the collision system, one must use the only available tools—the species and momenta of the particles which exit the collision region. Because of the violence of heavy-ion collisions, it is highly improbable for a nuclear cluster near center-of-mass rapidity ($y_{\mathrm{c.m.}}=1.6$) in a collision at these energies to be a fragment of the beam or target nucleus [1].

*Present address: Vanderbilt University, Nashville, TN 37235.
†Present address: Istituto di Cosmo-Geofisica del CNR, Torino, Italy and INFN Torino, Italy.
‡Present address: Anderson Consulting, Hartford, CT 06103.
§Present address: University of Denver, Denver, CO 80208.
‖Deceased.
¶Present address: Argonne National Laboratory, 9700 S. Cass Ave., Argonne, IL 60439.
**Present address: Cambridge Systematics, Cambridge, MA 02139.
††Present address: McKinsey & Co., New York, NY 10022.
‡‡Present address: Department of Radiation Oncology, Medical College of Virginia, Richmond, VA 23298.
§§Present address: University of Tennessee, Knoxville, TN 37996.
‖‖Present address: Geology and Physics Dept., Lock Haven University, Lock Haven, PA 17745.
¶¶Present address: Institut de Physique Nucléaire, F-91406 Orsay Cedex, France.
[a]Present address: Institute for Defense Analysis, Alexandria, VA 22311.
[b]Present address: MIT Lincoln Laboratory, Lexington, MA 02420-9185.
[c]Present address: Brookhaven National Laboratory, Upton, NY 11973.

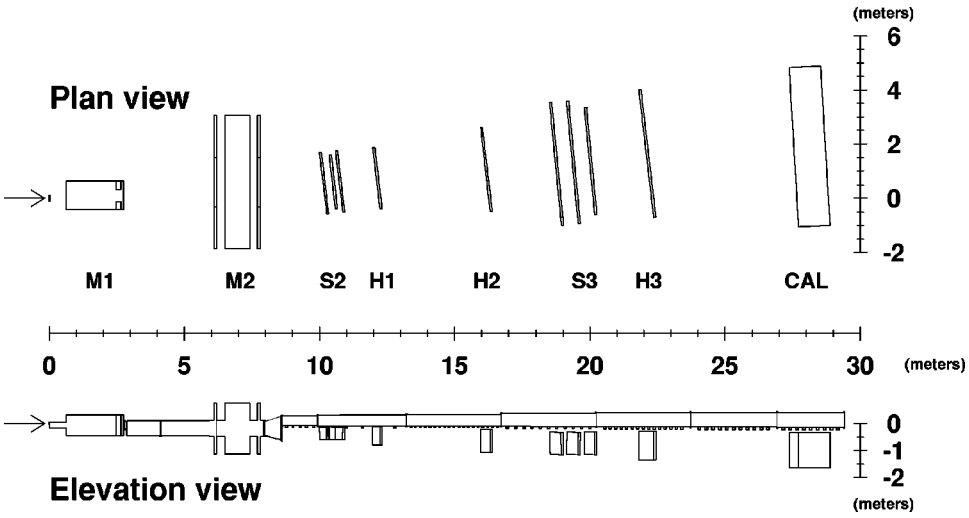

FIG. 1. The E864 spectrometer in plan and elevation views, showing the dipole magnets (M1 and M2), hodoscopes (H1, H2, and H3), straw tube arrays (S2 and S3), and hadronic calorimeter (CAL). The vacuum chamber is not shown in the plan view. The arrow shows the incident Au beam.

This would involve a cluster suffering a momentum loss of several GeV/c per nucleon that does not destroy the cluster, which is typically bound by only a few MeV per nucleon. These nuclei then are formed by coalescence and so represent correlations of several nucleons. As the mass of measured nuclei increases, so does the number of particles involved in the correlation and so does the sensitivity to features of the freeze-out distribution.

In part due to the fragility of these states, the observedlight nuclei are believed to be formed only near freeze-out of the collision system, at which time the mean free path of a bound cluster is long enough for it to escape without further collision. We have previously reported measurements of yields of stable light nuclei up to $A=7$ in collisions of ^{197}Au with beam momentum of 11.5A GeV/c on ^{197}Pt and ^{208}Pb targets and have discussed the trends of these measurements [2–4]. At AGS energies many measurements exist of particle spectra for single and composite hadrons in heavy-ion collisions [5]. Measurements of the yields of particle unstable nuclei can provide further insight into the evolution of the collision environment. We designate the resonant states measured here as ''particle unstable'' to distinguish them from nuclei which are stable or decay by weak interaction. In the discussion below, any nucleus with a lifetime long compared to the time to traverse the E864 apparatus ($\approx$100 ns) will be designated ''stable.''

In this paper we present measurements of the yields of the particle unstable nuclei ^{4}H, ^{4}Li, ^{5}He, and ^{5}Li and limits for the yields of two excited states $^5\mathrm{He}^*_{16.75\ \mathrm{MeV}}$ and $^5\mathrm{Li}^*_{16.66\ \mathrm{MeV}}$ in the 10% most central collisions of ^{197}Au with beam momentum of 11.5A GeV/c on ^{197}Pt. These are compared to the trends observed in the stable nuclei yields. We note that the widths of these unstable states (less than a few MeV/c^2) give lifetimes $c\tau \gtrsim 40$ fm, which means most produced nuclei decay outside of the collision volume.

II. EXPERIMENT 864

A. Apparatus

E864 uses an open geometry two-dipole spectrometer designed for high-sensitivity searches for exotic and rare composite objects. The apparatus (Fig. 1) has been described in detail elsewhere [6], so only the key items for this analysis will be described here. The 11.5A GeV/c beam of Au ions is incident on a 1.5-cm-thick Pt target (60% interaction length for Au). Beam definition counters and a scintillation multiplicity array [7] near the target form the first-level trigger for the experiment. Downstream of the dipole magnets, scintillation counter hodoscopes and straw tube arrays [8] provide time of flight (TOF), energy loss, and position measurements which allow off-line calculation of the charge, velocity, and rigidity of charged particles and thus the mass, momentum, and species. A highly segmented scintillating fiber and lead hadronic calorimeter [9] at the downstream end of the experiment allows an independent measurement of the TOF and energy for charged particles and identification of neutral particles. The tower-by-tower correlated TOF and energy from the calorimeter are used to make a second-level high-mass trigger (LET) [10]. The LET trigger can reject interactions with no high-mass particle in the spectrometer by a factor of 50–70.

Data from two separate runs are used for the analysis presented here. For both sets the first-level trigger selected the 10% most central interactions. A large data sample was recorded at the highest spectrometer field (1.5 T) with a primary goal of searching for strange quark matter. At this field setting the majority particles (p, π) are swept out of the spectrometer aperture. There is still moderate acceptance for ^{4}He and ^{3}H ions and good acceptance for neutrons. With these settings 250×10^6 LET triggers were recorded which sampled 13×10^9 10% most central interactions. This set of data is used for the ^{4}H and ^{5}He measurements. A second set of data was recorded at a lower field setting (0.45 T) with good acceptance for protons and all light ions. At this setting 45×10^6 LET triggers were recorded which sampled 1.9×10^9 10% most central interactions. This data set is used for the ^{4}Li, ^{5}Li, and excited state analysis.

B. Data analysis

Single-particle species are identified by using the charge and mass calculated from rigidity, energy loss, and TOF for

charged particles and the mass calculated from the TOF and energy in the calorimeter for neutral particles. Details of the particle identification and resolution are given in previous papers [2,3,6]. The particle unstable nuclei are identified by their decay into two daughter particles:

$$^4\mathrm{H} \rightarrow {}^3\mathrm{H} + n,$$

$$^4\mathrm{Li} \rightarrow {}^3\mathrm{He} + p,$$

$$^5\mathrm{He} \rightarrow {}^4\mathrm{He} + n,$$

$$^5\mathrm{Li} \rightarrow {}^4\mathrm{He} + p,$$

$$^5\mathrm{He}^*_{16.75\ \mathrm{MeV}} \rightarrow {}^3\mathrm{H} + d,$$

$$^5\mathrm{Li}^*_{16.66\ \mathrm{MeV}} \rightarrow {}^3\mathrm{He} + d.$$

For a given unstable nucleus events are selected which have at least one identified daughter of each type. Both particles are required to pass track or shower quality cuts and be consistent with coming from the target within the experiment's aperture. All pairs are used to calculate an invariant mass spectrum. Since most entries in this spectrum are uncorrelated background, one must determine the shape of the background spectrum. This is done by combining daughter particles of one type from one event with daughter particles of the other type from another event (event mixing) to form a mixed event invariant mass spectrum.

An additional cut requires the particles of a pair in both the same event spectrum and the mixed event spectrum to be separated by more than the two-track resolution in the relevant detectors. For charged pairs the cut is adjusted to be well beyond the observed two-track resolution in the tracking detectors. This resolution is set by the width of the slats in the scintillation counter hodoscopes (1.1 cm in H1, 1.5 cm in H2, and 2.3 cm in H3). The cuts used are 5 cm at H1, 6 cm at H2, and 7.5 cm at H3. The calorimeter is not used in the analysis of charged pairs, but is is used in the trigger. The trigger uses the correlation between the energy and time from each calorimeter tower to select events more likely to contain heavy particles. An additional requirement imposed off line that the two tracks be separated by more than 30 cm in either the horizontal or vertical direction at the calorimeter assures that there is no correlation in the same event pairs due to the trigger which would not be present in the mixed event pairs. A single calorimeter module is 10 cm horizontal by 10 cm vertical.

For pairs with one charged and one neutral particle, the neutral particle was required to be on one side of the detector (horizontally) and the charged particle on the other side with the two sides assigned to give optimum efficiency for simulated decays and the separation between the two sides larger than the two-shower resolution in the calorimeter. The two-shower resolution is set by contamination cuts used in the off-line shower analysis which tended to eliminate close pairs of showers up to a maximum distance of 30 cm vertically or horizontally. The minimum distance between the two sides of the detector used in this analysis is 30 cm.

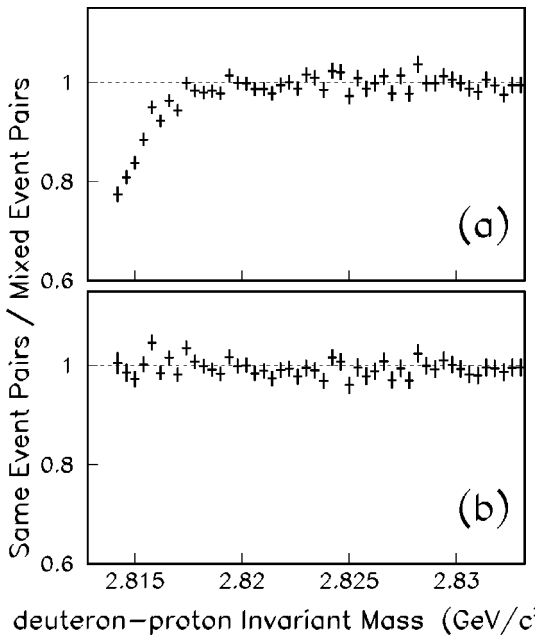

FIG. 2. Determination of the Coulomb correction from the deuteron-proton invariant mass spectrum. Panel (a) shows the ratio of the same event to mixed event mass spectrum with no correction. Panel (b) shows the same with the Coulomb correction.

For pairs where both particles are charged the mixed event invariant mass spectrum is modified to simulate the Coulomb interaction of the pair, so it will be canceled by subtraction from the same event spectrum. The form of the Coulomb interaction is taken to be a simple formula suggested by Baym and Braun-Munzinger [11]:

$$\frac{q^2}{2m_{red}} = \frac{q_0^2}{2m_{red}} + \frac{Z_1 Z_2}{r_0}, \tag{1}$$

where q_0 is the measured relative momentum of the pair, q is the modified relative momentum, m_{red} is the reduced mass, and Z_1 and Z_2 are the charges of the two particles. The one parameter r_0 which accounts for the average distance between the particles in the pair at freeze-out is determined as illustrated below from the deuteron-proton invariant mass spectrum where no other significant correlations are expected. Figure 2 shows the ratio of the deuteron-proton invariant mass spectrum for same event pairs to mixed event pairs without the Coulomb correction [Fig. 2(a)] and with the Coulomb correction [Fig. 2(b)] using the value $r_0 = 3.7$ fm which is the best fit to give a flat ratio after the correction. We note that the shape in Fig. 2(a) is dominated by our resolution. The maximum shift in q for the Coulomb correction used here is at $q = 0$ and is 22 MeV/c while our resolution in q is 35 MeV/c. Modification to the subtracted spectrum from the Coulomb interaction of the particles in a pair with the field of all the other particles is ignored. This interaction affects the single-particle distributions and should largely cancel in the subtraction. Although other treatments of the Coulomb correction have been published ([12], for

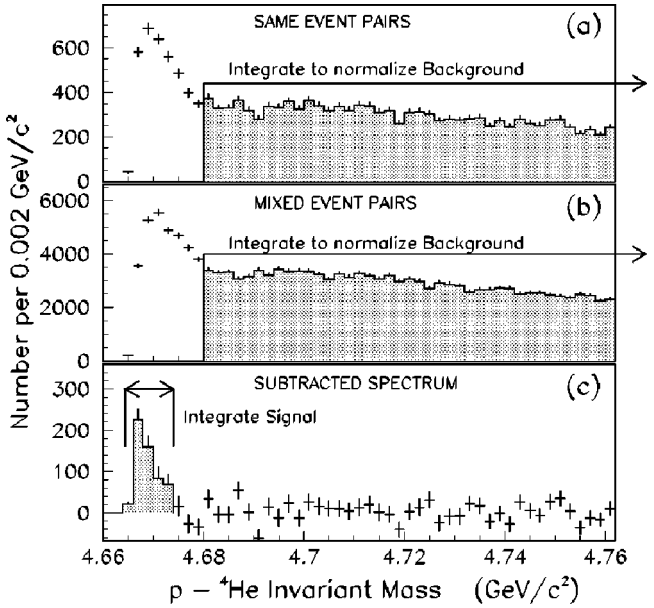

FIG. 3. Illustration of first method of mixed event analysis. Panel (a) shows the invariant mass spectrum for same event p-^{4}He pairs. Panel (b) shows the invariant mass spectrum for mixed event p-^{4}He pairs. Both spectra are for pairs in the rapidity range $2.0 \leqslant y \leqslant 2.2$ and $0.1 \leqslant p_T/A \leqslant 0.4$ GeV/c. The shading in both shows the region integrated to normalize the mixed event spectrum to the same event spectrum. Panel (c) shows the result of subtracting the normalized mixed event spectrum from the same event spectrum. The shading shows the region summed to count the ^{5}Li signal.

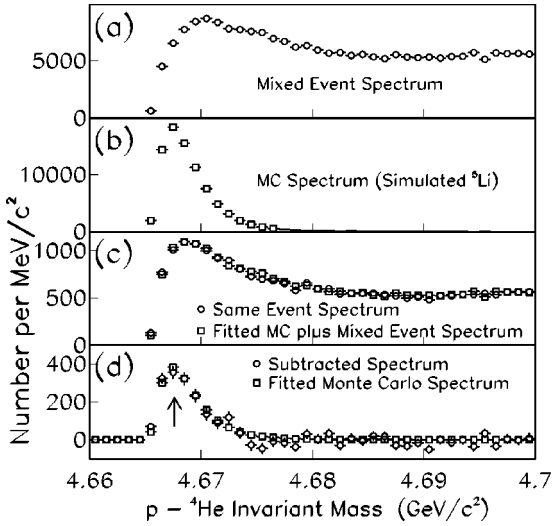

FIG. 4. Illustration of second method of mixed event analysis. Panel (a) shows the invariant mass spectrum for mixed event p-^{4}He pairs with a correction to simulate the Coulomb interaction. Panel (b) shows the Monte Carlo simulated signal for ^{5}Li. Panel (c) shows the same event mass spectrum (circles) overlayed with the sum of the Monte Carlo resonance spectrum plus the mixed event spectrum normalized with the parameters from a linear fit to the same event spectrum as described in the text (squares). Panel (d) shows the result of subtracting the normalized mixed event spectrum from the same event spectrum (circles) with the normalized Monte Carlo spectrum overlayed (squares). The arrow shows the nominal ^{5}Li mass. The plots include data from the full rapidity range to decrease the statistical error so that fine binning may be used to see the shapes.

example), since the shape in our data is dominated by our resolution, this simple parametrization is adequate for the analysis presented here.

At this point, the shape of the mixed event spectrum is assumed to represent the shape of the uncorrelated background plus the Coulomb interaction in the same event spectrum. However, the relative normalization of the two spectra is still unknown. The mixed event spectrum is normalized to the same event spectrum to extract the signal in two ways. In the first method the mixed event spectrum is normalized to the same event spectrum in a mass region above the expected signal. This is illustrated in Fig. 3 where the top and middle panels show the same event invariant mass spectrum and the mixed event spectrum (with Coulomb correction) for the ^{5}Li data sample in the rapidity range $2.0 \leqslant y \leqslant 2.2$ and $0.1 \leqslant p_T/A \leqslant 0.4$ GeV/c. We typically mix the tracks from one event with several other events so that the statistical error in the subtracted spectrum will be dominated by the number of pairs in the same event spectrum. To obtain the normalization between the same event and mixed event spectra, the bin contents for each spectrum are summed from 4.68 GeV/c^2 to the highest mass entry (well off the plot in Fig. 3) as indicated by the shaded region in Figs. 3(a) and 3(b). The ratio of these sums is used to scale the mixed event spectrum (middle panel) and the scaled mixed event spectrum is then subtracted bin by bin from the same event spectrum. The resulting subtracted spectrum should display the desired ^{5}Li signal and is shown in the bottom panel in Fig. 3. The shaded region in the bottom panel in Fig. 3 is integrated to count the number of ^{5}Li in this rapidity and transverse momentum bin.

The second method is illustrated in Fig. 4. Same event and mixed event invariant mass spectra are generated as in the first method. Additionally, an invariant mass spectrum is generated by using Monte Carlo generated resonance decays which are simulated through the entire apparatus (including detector resolution) and reconstructed. The top panel in Fig. 4(a) shows the mixed event spectrum from the data and Fig. 4(b) the Monte Carlo simulated ^{5}Li spectrum. A linear sum of the Monte Carlo spectrum [Fig. 4(b)] and the mixed event spectrum [Fig. 4(a)] is fitted to the same event spectrum [Fig. 4(c), circles]. Figure 4(c) (squares) shows the result of this two-parameter fit overlayed on the same event spectrum. To see the signal more clearly one can subtract the mixed event spectrum scaled according to the fit from the same event spectrum. This is shown in Fig. 4(d) (circles) where the Monte Carlo spectrum scaled according to the fit is overlayed (squares). The signal is integrated in the subtracted spectrum as in the first method. We have included data from the full rapidity and transverse momentum range used in the analysis in Fig. 4 to improve the statistics so as to be able to use finer binning to compare the signal shape from the data to the Monte Carlo signal shape. For the results presented in this paper, the two methods agree well within statistical error. We note that the signal width in Fig. 4 is dominated by our resolution. Reconstructing Monte Carlo simulated ^{5}Li decays including the detector resolution gives an invariant

TABLE I. Acceptances in percent for ^{5}Li decays with a magnetic field of 0.45 T. The first line is the total acceptance. The second line is the acceptance for a ^{5}Li decay when the ^{4}He is inside the calorimeter trigger region. These are typical of the acceptance for the data reported here.

Rapidity	1.7	1.9	2.1	2.3
Acceptance (%) for ^{5}Li	1.8	4.4	7.7	10.0
Acceptance (%) for ^{5}Li when ^{4}He is in the calorimeter trigger region	26.1	43.7	61.7	73.0

mass peak with a width of 4 MeV/c^2 [full width at half maximum (FWHM)] while the natural width is $\Gamma = 1.5$ MeV/c^2 [13].

Mass spectra are made for all rapidity bins with enough data to see a signal. As a result of the limited statistics, data are combined over a transverse momentum range of approximately $0.1 \leqslant p_T/A \leqslant 0.4$ GeV/c. To compare the yield of unstable nuclei ($Y_{unstable}$) to the yield of the species of the heavy decay daughter (Y_{Heavy}) we measure the number per collision, $N(y,p_t)$, of each in a given rapidity bin (Δy) and in a p_t range (Δp_t) centered about (y,p_t). The invariant multiplicity is given by

$$Y(y,p_t) = \frac{1}{2\pi p_t}\frac{N(y,p_t)}{\Delta p_t \Delta y}. \tag{2}$$

The ratio is given by

$$\frac{Y_{unstable}(y,p_t)}{Y_{Heavy}(y,p_t^*)} = \frac{N_{unstable}(y,p_t)}{N_{Heavy}(y,p_t^*)}\left(\frac{m_{Heavy}}{m_{unstable}}\right)^2 \times \frac{1}{\text{accept}(y,p_t)\times \text{effic}(y,p_t)\times \eta_{targ}}, \tag{3}$$

where accept(y,p_t) and effic(y,p_t) are the acceptance and efficiency for the light daughter when the heavy daughter has been accepted and the unstable parent is in the bin (y,p_t). As is the practice in calculating the invariant coalescence factors B_A, we wish to compare the spectra at similar velocities since the constituent particles must be close in velocity to coalesce. Thus we take the ratios in the same rapidity bin and with the p_t bin width and center for the heavy decay daughter, p_t^*, Δp_t^*, scaled from those of the unstable parent by the ratios of the masses of the two nuclei [see, for example, [14], Eq. (1.1) and the following text]. Finally, η_{targ} is the calculated target absorption for the light daughter. In this ratio, the trigger efficiency, acceptance, detector efficiency, and target absorption of the heavy decay daughter cancel.

Table I shows the acceptance for ^{5}Li decays in the kinematic range accessible for the 0.45-T spectrometer field setting. Also shown is the acceptance for ^{5}Li decays when the decay ^{4}He is in the region of the calorimeter used for the level II trigger for this data set. These values are typical for the acceptance for the unstable nuclei reported here.

For charged light daughters the efficiency includes detector and cut efficiencies (from data ≈ 0.8) and occupancy efficiency due to loss of the light daughter from overlapping tracks (from Monte Carlo tracks embedded in real events ≈ 0.7). For neutral light daughters (neutrons), the combination of cut efficiencies and loss due to overlapping showers in the calorimeter is calculated from embedding simulated showers in a real event (≈ 0.3 combined efficiency). A correction is made using the Monte Carlo resonance shape for loss of signal outside the mass region used for the signal which varies from $\approx 5\%$ in the lowest-rapidity bin to $\approx 10\%$ in the highest-rapidity bin. For the $A=5$ ground states, a correction is also made for ^{3}He contamination of the ^{4}He by extrapolating the ^{3}He shape under the ^{4}He peak. This correction is field and rapidity dependent, varying from less than 1% in the low-rapidity bin ($1.6 \leqslant y \leqslant 1.8$) to 16% at the high-rapidity bin and low-field setting ($2.2 \leqslant y \leqslant 2.4$ and 0.45 T). All these corrections are calculated as a function of rapidity and in the same p_T/A range used for the analysis.

Systematic errors that we have characterized include variation of the calculated acceptance with assumed production model ($\pm 15\%$ in the lowest-rapidity bin to $\pm 3\%$ in the highest), uncertainty in the correction for contamination of ^{4}He by ^{3}He for ^{5}He and ^{5}Li (only significant in the highest-rapidity bin, $\pm 8\%$), and uncertainty in the Coulomb correction for charged pairs ($\pm 5\%$ to $\pm 15\%$ depending on species and rapidity bin). To estimate possible systematic errors in calculating the acceptance due to the uncertainty in the shape of the production spectrum, we used several variations of the production model. We characterize the production by a Boltzman distribution in m_t and a parabolic shape in rapidity (y): $dN/dy = a + b(y - y_{\text{c.m.}})^2$. This parametrization describes our previously measured spectra for stable nuclei produced in these collisions [2]. We varied the inverse slope (T) in the Boltzman distribution from 60A to 180A MeV and varied the concavity of the rapidity distribution (b/a in above expression for dN/dy) from 0 (flat) to 12. We note that in the m_t and rapidity range of our measurements the observed rapidity concavity for the stable nuclei ranges from 0 for $A=1$ to 3 for $A=4$, increasing with A. We also used a model with a Gaussian variation of the inverse p_t slope with rapidity: $T = 112 + 117Ae^{-(y-y_{\text{c.m.}})^2/2\sigma^2}$ (MeV) with width $\sigma = 1.1$. For all these variations, the calculated acceptance varied by $\pm 3\%$ to $\pm 15\%$ of itself depending on rapidity bin and species.

For ^{4}Li and ^{4}H we note that the widths of the reconstructed invariant mass peaks are narrower than the value given in Ref. [13]. For example, for ^{4}Li the width that we observe is consistent with our resolution for a zero-width peak (≈ 3.5 MeV/c^2 FWHM). We conclude that the width is less than ≈ 3 MeV/c^2 which is consistent with other measurements (e.g., [15,16]). The value of this width slightly affects the acceptance and the correction for signal lost out-

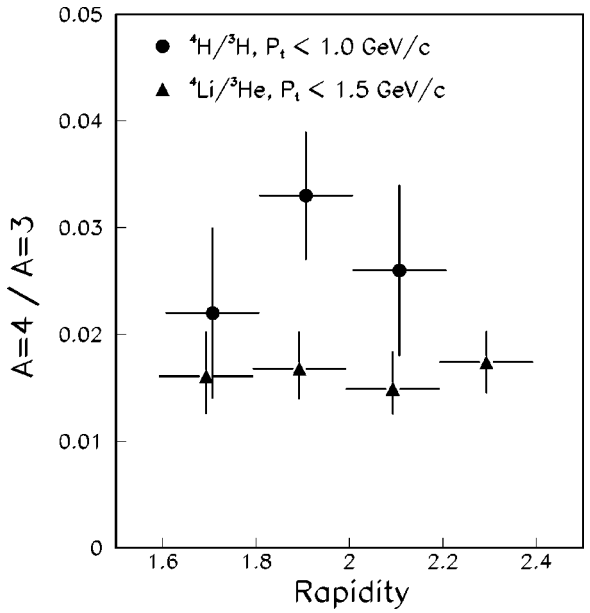

FIG. 5. Ratios of invariant multiplicities of $A=4$ unstable nuclei to invariant multiplicities of the heavy decay daughter species. Data points for different species are offset slightly from rapidity bin centers for clarity.

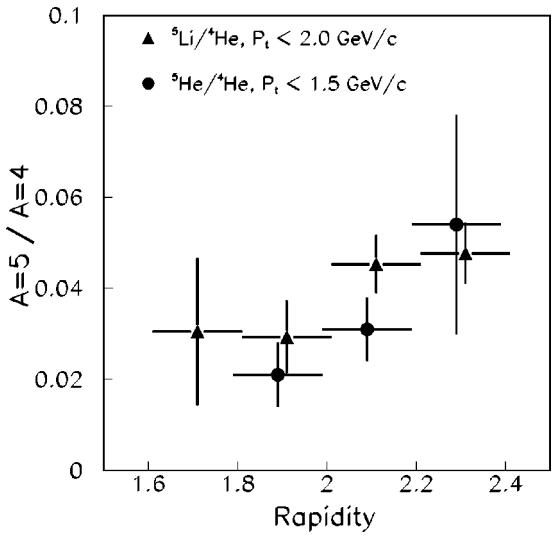

FIG. 6. Ratios of invariant multiplicities of $A=5$ unstable nuclei to invariant multiplicities of the heavy decay daughter species. Data points for different species are offset slightly from rapidity bin centers for clarity.

side the mass region integrated to count the signal. For the ^{4}Li results presented here, a width of 2 MeV/c^2 is used, and an additional systematic error of $\pm 3\%-5\%$ is included which covers a possible variation in width from 1 to 3 MeV/c^2. For the data presented here, the total estimated systematic error is added in quadrature to the statistical error. No corrections have been made for possible contributions to the mass peaks from excited states. We note that if these higher states are produced just in proportion to their spin factors, then they would represent $\approx 50\%-60\%$ of the measured $A=4$ yield and $\approx 13\%-17\%$ of the measured $A=5$ yield.

For the two excited states where we see no signal the total error, including statistical errors, systematic errors, and errors on the branching ratios [17,18] added in quadrature, is used to estimate a 90% confidence level upper limit for the yields.

III. RESULTS AND DISCUSSION

The ratios of invariant multiplicities for ^{4}H/^{3}H, ^{4}Li/^{3}He, ^{5}He/^{4}He, and ^{5}Li/^{4}He are shown in Figs. 5 and 6. We use the previously reported invariant multiplicities [2] to convert these ratios to the invariant multiplicities shown in Figs. 7 and 8. Included in Fig. 7 for comparison are the invariant multiplicities for ^{4}He from Ref. [2] averaged over the p_T range used here. Also shown in Fig. 8 are the 90% confidence level upper limits for the two $A=5$ $(3/2^+)$ excited states. The ratios and calculated multiplicities and errors are also given in Table II.

Some interesting features are evident from these figures. The invariant multiplicities for the $A=4$ unstable nuclei are within 50% of the invariant multiplicity for ^{4}He even though the spin factor for the unstable nuclei is 5 $(J=2)$ while it is only 1 $(J=0)$ for ^{4}He. There are no stable $A=5$ nuclei to compare with the unstable states, but they can be compared to the trends observed for the stable nuclei. Figure 9 shows the invariant multiplicities for ten stable nuclei at low p_t $(p_t/A \leqslant 300$ MeV/$c)$ and $1.8 \leqslant y \leqslant 2.0$ [2] along with the measurements for the four unstable nuclei and limits for the two excited states reported here. All multiplicities in this figure have been divided by $(2J+1)/2$ (spin factor normalized to protons) so as to allow a more direct comparison. The $A=7$ points which were measured in different rapidity bins have been shifted by a correction factor extrapolated from the rapidity shapes of the lighter nuclei ($\times 0.61$ for ^{7}Li and $\times 0.90$ for ^{7}Be). The exponential curve is fitted to the stable

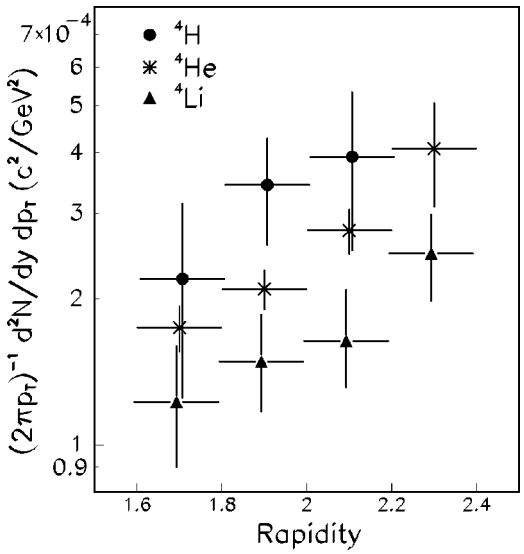

FIG. 7. Invariant multiplicities of $A=4$ nuclei. Data points for different species are offset slightly from rapidity bin centers for clarity.

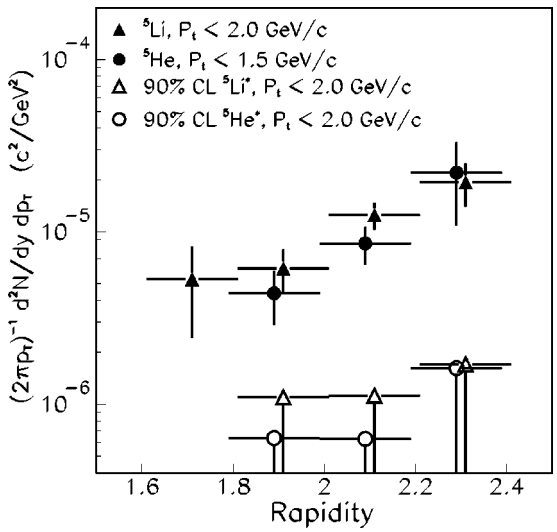

FIG. 8. Invariant multiplicities of $A=5$ nuclei and upper limits for the two excited states. Data points for different species are offset slightly from rapidity bin centers for clarity.

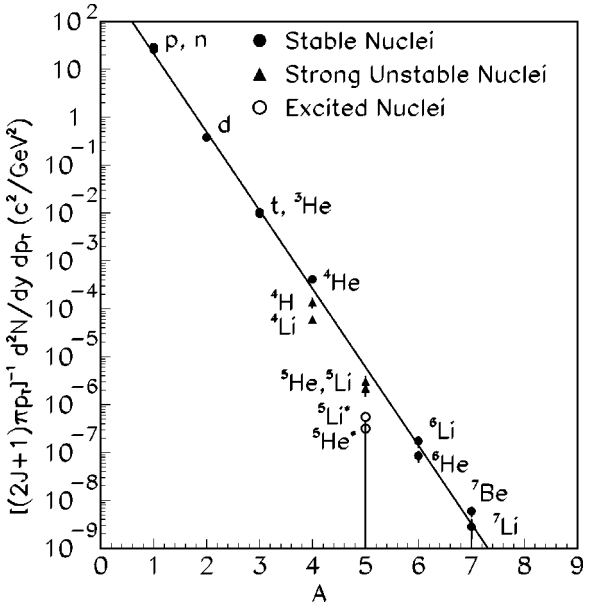

FIG. 9. Invariant multiplicities divided by $(2J+1)/2$ for stable and unstable nuclei in the range $1.8 \leqslant y \leqslant 2.0$. For the unstable nuclei and ^{6}He, $p_t/A \leqslant 400$ MeV/c. For the remaining nuclei, $p_t/A \leqslant 300$ MeV/c. The curve is an exponential fitted to the stable nuclei.

nuclei. The unstable nuclei follow the general exponential fall with increasing A that is seen in the stable nuclei, but are significantly below the level indicated by the fitted exponential. The ratios of the measured yields to the fitted curve are 0.36 ± 0.12 for ^{5}He and 0.50 ± 0.15 for ^{5}He.

Since the mass difference between the stable and unstable $A=4$ nuclei (≈ 23 MeV) is small compared to the temperatures of these collisions at freeze-out (≈ 100 MeV or greater) [19], a thermal model [20] would lead one to expect that the yields (scaled by the spin factor) would be similar. Thermal models generally give yields integrated over kinematic variables but our measurements are over a certain range in rapidity and p_T. Given the large difference when corrected for the spin factor between the stable and unstable $A=4$ multiplicities, however, and the fact that the ratios of the unstable to stable states vary by less than 25% from their average over the large rapidity region covered, it is not possible to ascribe the difference to the high-p_t region not measured in our experiment.

The yields of the $A=5$ excited states are significantly below the ground state yields. In many lower-energy experiments, the ratio of yields of these excited states to the ground states has been used to determine the temperature of the system produced in the collision [21]. This method is not expected to be valid when the temperature is much greater than the excitation energy of the excited state. It is interesting to note, however, that the upper limits on the production of the two $A=5$ excited states would imply a temperature lower

TABLE II. Ratios of the invariant multiplicity of the unstable nucleus to the invariant multiplicity of the species of its heavy decay daughter and the invariant multiplicities calculated using previously reported yields for the species of the heavy decay daughter. For the excited states, $^5\mathrm{He}^*_{16.75\ \mathrm{MeV}}$ and $^5\mathrm{Li}^*_{16.66\ \mathrm{MeV}}$ the 90% confidence level upper limit is given.

	Ratios to heavy decay daughter			
Rapidity	1.7	1.9	2.1	2.3
^{4}Li/^{3}He	0.016 ± 0.004	0.017 ± 0.003	0.015 ± 0.003	0.017 ± 0.003
^{4}H/^{3}H	0.022 ± 0.008	0.033 ± 0.006	0.026 ± 0.008	
^{5}Li/^{4}He	0.031 ± 0.017	0.029 ± 0.008	0.045 ± 0.007	0.048 ± 0.009
^{5}He/^{4}He		0.021 ± 0.007	0.031 ± 0.007	0.054 ± 0.021
	Invariant multiplicities $\times 10^5$ (c^2/GeV^2)			
^{4}Li	12 ± 2	15 ± 2	16 ± 1	25 ± 2
^{4}H	22 ± 10	34 ± 9	39 ± 14	
^{5}Li	0.53 ± 0.29	0.61 ± 0.18	1.3 ± 0.2	1.9 ± 0.5
^{5}He		0.44 ± 0.15	0.86 ± 0.21	2.2 ± 1.1
$^5\mathrm{Li}^*_{16.66\ \mathrm{MeV}}$ (90% C.L. upper limit)		0.11	0.11	0.17
$^5\mathrm{He}^*_{16.75\ \mathrm{MeV}}$ (90% C.L. upper limit)		0.06	0.06	0.16

than 7–13 MeV ($y=2.3$–$y=1.9$) if interpreted in this way. Since temperatures at these energies have been previously measured to be ≈ 100 MeV or greater, it is highly unlikely that nucleons at a temperature of ≈ 100 MeV would coalesce into resonant nuclei with temperatures this low. A more consistent interpretation of the lower yields of excited and unstable states may come from a coalescence model such as that of Scheibl and Heinz [14] which explicitly includes the internal structure of the formed cluster. In particular, their quantum-mechanical correction factor which would be 1.0 for the production of point particles becomes increasingly smaller as the size of the coalesced system approaches (or exceeds) the size of the region of homogeneity for the collision (given, for example, by HBT radii). Scheibl and Heinz calculate that for deuteron production in Au-Au collisions at SPS energies this correction factor is 0.66–0.86 for a variety of collision fireball parameters and deuteron wave functions. Scheibl and Heinz use a deuteron rms radius of 1.96 fm and radii of homogeneity of $R_{||}(m_t=1\ \mathrm{GeV}/c^2)=3.2$ fm and $R_{\perp}(m_t=1\ \mathrm{GeV}/c^2)=5.1$ fm.

Direct measurements of radii for the particle unstable nuclei reported here are not possible; however, circumstantial evidence suggests these nuclei are large. The states are unbound and typically have very large resonant cross sections. For example, the n-^{4}He cross section is about 7 b at resonance [22]. The recent availability of radioactive beams has allowed measurement of the interaction cross sections of metastable halo nuclei from which one may deduce a radius. For ^{14}Be, for example, Suzuki *et al.* [23] determine an rms radius of 3 fm and a valence radius (core to halo) of 5 fm. Scheibl and Heinz have not made calculations for nuclei above $A=3$; however, they do include a calculation for deuterons produced from p-p interactions. Using a radius of homogeneity of about 1 fm compared to the deuteron radius of 1.96 fm, they obtain a value for their correction factor of 0.15. Again, this factor would be 1.0 if the deuteron were a point particle. It seems quite possible then that the large size of the unstable states accounts for the suppression in coalescence yield compared to the stable nuclei. To make this statement quantitative, however, will require a detailed calculation including the nuclear wave functions.

We note that data are now available for yields of coalesced nuclei from heavy-ion collisions at AGS energies up to $A=7$. Others have pointed out that coalescence yields represent correlations of the coalesced nucleons and can give complementary information to the correlations studied with HBT analyses [24,25]. Detailed calculations including nuclear wave functions, although difficult, can provide more information about the density profile of the collision at freeze-out.

IV. SUMMARY

We have measured the yields of four unstable nuclei ^{4}H, ^{4}Li, ^{5}He, and ^{5}Li in 11.5A GeV/c Au+Pt 10% most central collisions in the rapidity range from $y_{\mathrm{c.m.}}$ to $y_{\mathrm{c.m.}}+0.8$ and in the transverse momentum range of approximately $0.1 \leqslant p_T/A \leqslant 0.4$ GeV/c. The invariant multiplicities in this kinematic range fall significantly below what would be expected from a simple thermal model based on the previously measured yields of stable nuclei. It is likely that a detailed calculation which includes the nuclear structure will show that this is expected for these large nuclei.

ACKNOWLEDGMENTS

We gratefully acknowledge the efforts of the AGS staff in providing the beam and support for the experiment. This work was supported in part by grants from the U.S. Department of Energy (DOE) High Energy Physics Division, the DOE Nuclear Physics Division, and the National Science Foundation.

[1] L. C. Alexa *et al.*, Phys. Rev. Lett. **82**, 1374 (1999); D. Abbott *et al., ibid.* **82**, 1379 (1999).
[2] T. A. Armstrong *et al.*, Phys. Rev. C **61**, 064908 (2000).
[3] T. A. Armstrong *et al.*, Phys. Rev. C **60**, 064903 (1999).
[4] T. A. Armstrong *et al.*, Phys. Rev. Lett. **83**, 5431 (1999).
[5] *Heavy Ion Physics From Bevalac To RHIC, Proceedings of the Relativistic Heavy Ion Symposium, APS Centennial Meeting '99*, Atlanta, 1999, edited by R. Seto (World Scientific, Singapore, 1999).
[6] T. A. Armstrong *et al.*, Nucl. Instrum. Methods Phys. Res. A **437**, 222 (1999).
[7] P. Haridas, I. A. Pless. G. Van Buren, J. Tomasi, M. S. Z. Rabin, K. Barish, and R. D. Majka, Nucl. Instrum. Methods Phys. Res. A **385**, 413 (1997).
[8] T. A. Armstrong, R. A. Lewis, J. Passaneau, G. A. Smith, J. D. Reid, J. Stell, and W. S. Toothacker, Nucl. Instrum. Methods Phys. Res. A **425**, 210 (1999).
[9] T. A. Armstrong *et al.*, Nucl. Instrum. Methods Phys. Res. A **406**, 227 (1998).
[10] J. C. Hill *et al.*, Nucl. Instrum. Methods Phys. Res. A **421**, 431 (1999).
[11] G. Baym and P. Braun-Munzinger, Nucl. Phys. **A610**, 286c (1996).
[12] Scott Pratt, Phys. Rev. D **33**, 72 (1985).
[13] *Table of Isotopes*, 8th ed., edited by Richard B. Firestone and Virginia S. Shirley (Wiley, New York, 1996).
[14] R. Scheibl and U. Heinz, Phys. Rev. C **59**, 1585 (1999).
[15] M. Bruno, C. Cannata, M. D'Agotino, and M. L. Fiandri, Phys. Rev. C **42**, 448 (1990).
[16] B. Brinkmoller, H. P. Morsch, P. Decowski, M. Rogge, R. Siebert, and P. Turek, Phys. Rev. C **42**, 550 (1990).
[17] D. R. Tilley, H. R. Weller, and G. M. Hale, Nucl. Phys. **A541**, 1 (1992).
[18] B. Haesner, W. Heeringa, H. O. Klages, H. Dobiasch, G. Schmalz, P. Schwarz, J. Wilczynski, and B. Zeitnitz, Phys. Rev. C **28**, 995 (1983).
[19] See, for example, P. Braun-Munzinger and J. Stachel, Nucl. Phys. **A606**, 320 (1996), and references therein.

[20] S. Das Gupta and A. Z. Mekjian, Phys. Rep. **72**, 131 (1981); P. Braun-Munzinger, J. Stachel, J. P. Wessels, and N. Xu, Phys. Lett. B **344**, 43 (1995).

[21] See, for example, C. Schwarz *et al.*, Phys. Rev. C **48**, 676 (1993); J. B. Natowitz, J. C. Hagel, R. Wada, X. Bin, J. Li, Y. Lou, and D. Utley, *ibid.* **48**, 2074 (1993), and references therein.

[22] S. Bashkin, F. P. Mooring, and B. Petree, Phys. Rev. **82**, 378 (1950).

[23] T. Suzuki *et al.*, Nucl. Phys. **A658**, 313 (1999).

[24] A. Polleri, J. P. Bondorf, and U. N. Mishustin, Phys. Lett. B **419**, 19 (1998).

[25] R. Mattiello, H. Sorge, H. Stöcker, and W. Greiner, Phys. Rev. C **55**, 1443 (1997).